ОБЪЕДИНЕННЫЙ
ИНСТИТУТ
ЯДЕРНЫХ
ИССЛЕДОВАНИЙ

Дубна

E14 - 3759

A. Holas, J. Holas, E. Maliszewski,
L. Sedlakova

FOCUSING OF THE TIME-OF-FLIGHT DIFFRACTOMETER FOR STRUCTURE ANALYSIS.

The Experimental Check

ЛАБОРАТОРИЯ НЕЙТРОННОЙ ФИЗИКИ

1968

E14 - 3759

A. Holas,* J. Holas, E. Maliszewski,*
L. Sedlakova **

FOCUSING OF THE TIME-OF-FLIGHT DIFFRACTOMETER FOR STRUCTURE ANALYSIS.

The Experimental Check

Submitted to Nuclear Instruments and Methods

---

*On leave from the Institute of Nuclear Research, Świerk, Poland.

**On leave from the Nuclear Research Institute, Řež, Czechoslovakia.

I. Introduction

The time-of-flight (TOF) method in the neutron diffractometry has been recently developed and used for crystal structure analysis/ 1/ .

A very high resolution is often required for experiments of this type. Usually all steps towards improving the resolution are accompanied by losses in intensity. For the case of the TOF neutronography a new method of focusing of the diffractometer - free of this disadvantage - has been recently proposed/ 2/ . In this paper the experimental check of the focusing method is presented. The experiments have been performed on the pulsed fast reactor IBR/ 3/ of the Joint Institute for Nuclear Research, Dubna, USSR.

II. The Principles of Focusing/ 2/

Let us consider a reflection from the crystal plane ($h\,k\,\ell$) of a powdered or single-crystal sample. The time of flight of a scattered neutron, t, is uniquely given by the expression:

$$t = L / v = L \lambda m / h , \tag{1}$$

where the wavelength λ is defined by the Bragg equation

$$\lambda = 2d_{hk\ell}\sin\theta , \tag{2}$$

and

L is the flight path of this neutron,

v is its velocity,

2θ is the scattering angle (the angle between directions of the neutron trajectories before and after scattering),

m is the neutron mass,

h is the Planck constant.

The finite dimensions of the source, the sample and the counter (SSC) cause a spreading of L and θ, and therefore a broadening of the peak. Let $t(\vec{r}_r, \vec{r}_s, \vec{r}_c)$ be the time of flight of the neutron which left the point $\vec{r}_r$ (see Fig. 1) of the source, was scattered (according to Bragg's law) at the point $\vec{r}_s$ of the sample, and was recorded at the point $\vec{r}_c$ of the counter. This function may be expanded in a Traylor series. (For the sake of convenience let us introduce the function r, the relative increase of time).

$$r(\vec{r}_r, \vec{r}_s, \vec{r}_c) = \frac{t(\vec{r}_r, \vec{r}_s, \vec{r}_c) - t(0,0,0)}{t(0,0,0)} = \vec{\rho}_r\vec{r}_r + \vec{\rho}_s\vec{r}_s + \vec{\rho}_c\vec{r}_c + \dots \tag{3}$$

where

$$\vec{\rho}_i = \frac{1}{t}\frac{\partial t}{\partial \vec{r}_i} , \qquad i = r, s, c .$$

Let us assume that the terms of the second and higher orders can be neglected. This is fulfilled when the linear dimensions of the SSC are small compared with the distances between them. Let us further treat the SSC as thin plates set perpendicularty to the vectors $\vec{\rho}_r, \vec{\rho}_s$ and $\vec{\rho}_c$, respectively (see Fig.2.) For such geometry the peak broadening due to the dimensions of the SSC is negligible (the maximal spreading of the reduced time

$$r_m = |\vec{\rho}_r| \cdot s_r + |\vec{\rho}_s| \cdot s_s + |\vec{\rho}_c| \cdot s_c \tag{4}$$

can be made sufficiently small for the small thicknesses s_r, s_s and s_c). Nevertheless the intensity of the peak remains high because the dimensions of the SSC perpendicular to $\vec{\rho}_r, \vec{\rho}_s, \vec{\rho}_c$ can be quite large. The diffractometer with such setting will be called <u>focused.</u> Substituting (1) and (2) into (3) we obtain the formulae for vectors $\vec{\rho}_i$:

$$\vec{\rho}_i = \frac{1}{t} \frac{\partial t}{\partial \vec{r}_i} - \frac{1}{L} \frac{\partial L}{\partial \vec{r}_i} + \cot\theta \frac{\partial \theta}{\partial \vec{r}_i} \tag{5}$$

$i = r, s, c,$

where functions t, L, θ and their derivatives are taken at the point $\vec{r}_r = 0$, $\vec{r}_s = 0$, $\vec{r}_c = 0$.

As an example we derive here the formula for $\vec{\rho}_r$. The increase of the flight path corresponding to the point (x_r, y_r, z_r) of the source is (see Fig.3):

$$\delta L = y_r \tag{6}$$

and the increase of the Bragg angle is

$$\delta\theta = \frac{1}{2}(2\theta - 2\theta_0) = \frac{1}{2} \frac{x_r}{L_r} . \tag{7}$$

Comparing (6) and (7) with (3) and (5) we obtain:

$$\vec{\rho}_r = (\xi_r, \eta_r, \zeta_r) = \left(\frac{\cot\theta_0}{2L_r}, \frac{1}{L_r + L_c}, 0 \right). \tag{8}$$

Similar consideration /2/ leads to the formulae:

$$\vec{\rho}_c = (\xi_c, \eta_c, \zeta_c) = \left(\frac{\cot\theta_0}{2L_c}, \frac{1}{L_c + L_r}, 0 \right), \tag{9}$$

$$\vec{\rho}_s = (\xi_s, \eta_s, \zeta_s) = \tag{10}$$

$$\left(\frac{2\sin\theta_0}{L_r + L_c} + \frac{1}{2}\cot\theta_0\cos\theta_0\left[\frac{1}{L_r} + \frac{1}{L_c}\right], \frac{1}{2}\cot\theta_0\sin\theta_0\left[\frac{1}{L_c} - \frac{1}{L_r}\right], 0\right),$$

where (see Fig. 1 and 2):

$2\theta_0$ is the angle between the directions 0_r0_s and 0_s0_c, respectively,

L_r, L_c are the distances 0_r-0_s and 0_s-0_c, respectively.

The scheme of the focused spectrometer is shown in Fig. 2. When the vectors $\vec{\rho}_i$ are known, it is easy to find the characteristic angles α_{i0} :

$$\tan\alpha_{i0} = \xi_i / \eta_i , \tag{11}$$

$$\tan\alpha_{r0} = \frac{1}{2}(1+p)\cot\theta_0, \tag{12}$$

$$\tan\alpha_{c0} = \frac{1}{2}(1+1/p)\cot\theta_0 , \tag{13}$$

$$\tan\alpha_{s0} = [4\tan\theta_0 + (2+p+1/p)\cot\theta_0]/(1/p - p), \tag{14}$$

where

$$p = L_c / L_r .$$

Formulae (12), (13) and (14) do not depend on the peak indices $(h\,k\,\ell)$, , what means that the focusing conditions can be satisfied <u>simultaneously for all the peaks.</u> It is also worthwhile to emphasize that the above considerations hold both for powdered samples and single crystals.

III. The TOF Diffractometer.

In order to prove the focusing formulae experimentally the neutron TOF diffractometer[4] at the IBR was partly reconstructed. The arrangement used in the described experiment is shown in Fig. 4. Fast neutrons from the reactor core (1), slowed down by a "poisoned"/5/ moderator (2), pass through a vacuum tube (3), are scattered on a sample (8) and then are registered by a scintillation counter (7). The scintillator is in a form of a vertical, thin (0.5 mm) rectangular plate 16 cm heigh and 50 cm wide. The construction of the shielding allows to turn the counter round the vertical axis going through the centre of the scintillator plate. The distance from the centre of the moderator to the sample centre, L_r, is 18.41 m, and that from the sample center to the counter centre, L_c, is 2.80 m. The mean power of the reactor was 3 kW.

All the measurements using silicon powder were performed with one sample containing about 240 g of powdered Si in an aluminium rectangular container (2 cm x 5 cm x 11 cm).

The results obtained with the focused diffractometer were compared with the measurement performed with a partly defocused diffractometer equipped with Soller collimators. For this purpose one 20-minutes collimator has been placed in the biological shielding (see (4) in Fig. 4) of the reactor, and another similar collimator has been placed between the counter and the sample. The surface of the counter was set perpendicularly to the direction from the centre of the counter to the centre of the sample. The sample was in a symmetrical reflection position. This set up was analogous to that described in paper/4/. We shall call it <u>the diffractometer with collimators.</u>

IV.Results Concerning Resolution

1. As can be seen from formulae (12), (13) and (14) the characteristic angles a_{r0}, a_{c0} and a_{s0} for the focused diffractometer are determined by the scattering angle $2\theta_0$ and by $p = L_c / L_r$. The scattering angle $2\theta_0$ was chosen to be 87° in order to work in a convenient range of wavelengths. In the described case the surface of the moderator (which play the role of a source of thermal neutrons) is not perpendicular to the neutron beam, but is declined by

the angle of 30° (see Fig. 4). Hence $\alpha_{r0} = 30^{\circ}$ was determined by the conditions being in the reactor hall. Consequently p (see formula (12)) is also determined and should be equal to 0.094 for the completely focused diffractometer. However, the conditions did not allow to satisfy this requirement and all the measurements have been made with $p = 0.15$. As can be easily calculated, this small deviation does not change the resolution in a measurable way. However it causes an appreciable loss of intensity (by a factor of $(0.15/0.094)^2 \approx 2.5$). The chosen value of $p = 0.15$ leads to $\alpha_{s0} = 63^{\circ}40'$ and $\alpha_{c0} = 76^{\circ}$ (fomulae (14) and (13)).

2. Following the discussion given in paper/6/ we use the variance D^2 of the reduced time of flight τ (see formula (3)) as a quantitive measure of the resolution of the ($h\,k\,\ell$) reflection:

$$D^2 = \overline{(\tau - \bar{\tau})^2}\ , \tag{15}$$

where the bar denotes averaging using the intensity distribution function. Since this distribution function may be expressed as a fold of distributions corresponding to independent contributions to the peak width, the resolution of the peak (variance) becomes the sum of the corresponding variances (partial resolutions). This useful property allows to calculate separately the partial resolutions corresponding to the source, the sample and the counter. In Appendix the formulae for the resolutions D_c^2 and D_s^2 (due to the dimensions of the counter and the dimensions of the sample, respectively) are derived as a function of the parameters describing the experiment.

The property of the additivity of the partial resolutions allows also to measure each partial resolution separately as a function of the parameters affecting only this partial resolution. For example in the case of D_c^2 one measures the total resolution D^2 as a function of α_c (the angle between the direction from the sample centre to the counter centre and the normal to the counter surface, see Fig. 2.).However,

$$D_c^2 = D^2 - D_{r,s}^2 \tag{16}$$

(where the contribution to the resolution from all the sources but the counter, $D^2_{r,s}$, is independent of α_0), which shows that D^2 and D^2_0 as functions of α_0 differ only by a constant.

3. In praxis the experimental resolution of the ($hk\ell$) reflection can be calculated using the formula:

$$D^2 = \sum_{n=n_f}^{n_\ell} N_n (n-\bar{n})^2 / (I\,\bar{n}^2), \qquad (17)$$

where

$I = \sum_{n=n_f}^{n_\ell} N_n$ is the intensity of this reflection,

$\bar{n} = \sum N_n\, n / I$ is the mean position (in channel number) of the peak,

N_n is the number of counts in the n-th channel, corrected for the background,

n_f, n_ℓ are the first and the last channel numbers belonging to the peak.

The larger is the number of channels ($n_\ell - n_f$) belonging to the peak, the better is the approximation of formula (15) by formula (17).

4. In order to check experimentally the focusing conditions for the counter (and, by the way, to prove the validity of formulae A2 and A3 derived in Appendix) measurements were performed for a set of inclination angles α_0. The results obtained for the powdered silicon sample are summarized in Fig. 5. The solid line was calculated using formula A2 for $\alpha_0 > 161^\circ$ and A3 for remaining α_0 and the parameters describing the experiment (see Section III, and $\omega_c = 0.24\,m / 2.8\,m$ caused by the counter shielding). The triangles and circles show the experimentally measured resolution D^2_0 (for the (220) and (111) reflections) with the help of formulae (17) and (16). The constant (in this case) value $D^2_{r,s}$ was obtained by applying the condition that the mean deviation of the experimental points from the theoretical curve (solid line) should be equal to zero. A good fit of the theoretical curve to the experimental points confirms the vali-

dity of formulae A2 and A3. The value of α_c for a minimum of D_c^2 agrees well with the calculated value $\alpha_{c0} = 76^0$ for the focusing condition.

5. Analogically the focusing conditions were checked for the sample. The obtained results are shown in Fig. 6. Here, α_s is the angular deflection from the symmetrical position in "transmission" ($\alpha_s = 90^0$ corresponds to the position in "reflection"). The solid line was calculated using formula A7 and the parameters describing the experiment. The experimental resolution D_s^2 due to the dimensions of the sample is marked with crosses for the (311) reflection and with traingles for the (220) reflection. It was obtained as the difference between the total resolution D^2 (calculated with the help of formula (17)) and the resolution due to the neutron source and the counter, $D_{t,c}^2$. The latter was found using the same procedure as for $D_{t,s}^2$ in the counter case. A good fit of the theoretical curve to the experimental points confirms the validity of formula A7. The minimum of D_s^2 agrees well with the calculated value $\alpha_{s0} = 63^0\,40'$ for the focusing condition.

6. By focusing the source, the sample and the counter we have removed the contribution to the width of the peak due to the SSC dimensions . Assuming that the remaining width of the peak is due only to the width of the neutron pulse, this partial resolution $D_{\delta t}^2$ can be measured experimentally. Fig. 8 shows the experimentally measured values of $D_{\delta t}^2$ as a function of the wavelength, obtained from reflections from various samples using the focused diffractometer. The solid line is described by the formula:

$$D_{\delta t}^2(\lambda) = \overline{\delta t^2} / t^2(\lambda), \qquad (18)$$

where $\overline{\delta t^2}$ is the mean value of the absolute resolution ($D_{\delta t}^2 \times t^2$) of all the experimental points. The big dispersion of the experimental points takes place mainly because the channel numbers in which the peaks end and the background begins are difficult and arbitrary to determine. Formula (17) is very sensitive to these quantities.

Therefore the only conclusion which may be drawn from these results is that the variance corresponding to the time width of the pulse is independent of λ within the limits of errors and equals

$$\overline{\delta t^2} = (4000 \pm 1500)(\mu\,\mathrm{sec})^2 .$$

where 1500 is the mean absolute deviation. A halfwidth of the peaks increases slightly from the value 100 μsec for $\lambda = 1.7$ Å to 130 μsec for $\lambda = 4.3$ Å .

7. Fig. 9. shows the comparison between the halfwidths obtained with the focused diffractometer (points marked with "f") and with the diffractometer with collimators x) (points marked with "c"). The (relative) halfwidths $D_{1/2}$ are practically the same for the two cases in the wavelength range up to 3.3 Å. For the longer wavelengths the resolution in the focusing case becomes better. These facts may be explained in the following way. In the case of the diffractometer with collimators the source remained focused. Hence the collimator between the source and the sample should not change the resolution, except in the range of $\lambda \gtrsim 3.3$ Å , where neutrons totally reflected by the lamellae of the collimator cause the broadening of the peaks (see Section V.3). The second collimator (of 20′ divergence) also did not practically change the resolution from the counter side, since its resolution is small as compared with the neutron pulse resolution ($= 10 \times 10^{-6}$ at 4 Å , see Fig. 8), except in the longest wave region, where the mentioned total reflections start to play the role. The contribution of the dimensions of the sample to the peak width becomes also important in the range of $\lambda \gtrsim 4$ Å , since the resolution due to it may be estimated as $(2 \div 4) \times 10^{-6}$ in the case of the sample used.

x) See the end of Section III.

V. Results Concerning Intensity

1. Fig. 10 shows the diffraction pattern obtained in 25 hours using the focused spectrometer, and Fig.11 shows the one obtained in 42 hours by means of the diffractometer with collimators. The silicon powder sample used was described in Section III. The great increase of intensity in the focused case is evident. The third line in Table 1 gives the ratio I_f / I_c of the investigated intensities I_f and I_c in the two cases, respectively (normalized to the same exposure time).

2. The obtained increase of intensity depends strongly on the wavelength. This is mainly due to the fact that the dependence of the counter efficiency on the wavelength changes with the angle α_c . In order to prove this assumption an additional experiment was performed. By means of single crystals (zinc and aluminium) monochromatic beams of several wavelengths were obtained. For each wavelength measurements have been performed for two positions of the counter (for $\alpha_c = 76^0$ and $\alpha_c = 0^0$). Fig. 12 shows the ratio of the two measured intensities as a function of λ . The angular dimensions of neutron beams reaching the counter were the same for both cases in this experiment. Therefore the measured ratio $I(\alpha_{c0})/ I(0^0)$ is equal to the corresponding ratio of the counter efficiencies. *

This result is easy to explain. The effective thickness of the scintillation layer increases $1/\cos\alpha_c$ times as compared with the thickness for $\alpha_c = 0$, when the counter is declined by the angle α_c. The fourth line in Table 1 gives the gain of intensity in the focused case corrected for the change of the counter efficiency shown in Fig. 12. Such an increase of intensity would be possible to obtain with a four times thinner scintillation layer.

3. The figures in the fourth line in Table 1 show still a weak dependence on the wavelength. It may be explained by the reflection of neutrons from collimator lamellae favoured for long wavelengths.

The transmission of a collimator with totally reflecting lamellae is greater than the transmission of the collimator with "black" lamellae by a factor

$$[1 + (\phi_c / a)^2] \quad \text{for} \quad \phi_c \leq a,$$

and

$$[2 \times \phi_c / a] \quad \text{for} \quad \phi_c \geq a,$$

where

ϕ_c is the critical angle,

a is the divergence of the collimator.

The transmission of a collimator increases with λ since $\phi_c \sim \lambda$. For iron lamellae used in the described experiment, $\phi_c = 5.5' \times \lambda / Å$. Going from $\lambda = 1.72$ Å to $\lambda = 4.33$ Å, this leads to the increase of intensity

$$I_c(4.33 \text{ Å}) / I_c(1.72 \text{ Å}) = 3.7 \,.$$

This number compared with the experimentally obtained gain $47/36 = 1.3$ (see fourth line in Table 1) shows, that the collimators used do not reflect neutrons ideally.

4. It may be of interest to know what differences between the two diffractometers are mainly responsible for the observed gain in intensity. Since both measurements were made with the same sample and the distances L_r and L_c were unchanged (which is important because of absorption in the air), it is enough to compare only the solid angles (divergences) of the beam incoming the sample and the beam scattered towards the counter/ 6/.

The beam coming from the source to the sample was limited by a tube (marked with (3) in the shielding (4) in Fig. 4) with radius of 0.10 m. The far end was at a distance of 13.1 m from the sample. The resulting solid angle is $\pi \times 0.10^2 / 13.1^2 = 1.8 \times 10^{-4}$. In the case of the diffractometer with collimators the horizontal divergence equals the collimator divergence $20' = 5.8 \times 10^{-3}$. The vertical divergence is defined by the height (0.11 m) of the collimator and the distance (12.8 m) from the far end of the collimator to the sample. So the total divergence is $5.8 \times 10^{-3} \times 0.11 / 12.8 = 0.50 \times 10^{-4}$. Hence the gain of intensity connected with the incoming beam is $1.8 / 0.5 = 3.6$.

The divergence of the scattered beam, reaching the counter, is defined in the focusing case by the dimensions of the counter: 0.16 m height, 0.5 m wide, inclined by the angle 76°, and placed at a distance of 2.80 m from the sample. The corresponding solid angle equals $(0.16 / 2.80) \times (0.5 \times \cos 76° / 2.80) = 0.057 \times 0.043 = 24 \times 10^{-4}$ In the case of the diffractometer with collimators, the far end of the collimator (the same as used in the biological shielding) was at a distance of 2.20 m from the sample. The resulting divergence is therefore $(0.11 / 2.20) \times 20' = 0.05 \times 0.0058 = 2.9 \times 10^{-4}$. So the gain of intensity connected with the scattering beam is $24 / 2.9 = 8.5$.

The estimated total increase of intensity is thus $3.6 \times 8.5 = 30$. This shows that the above calculations reflect properly the main reasons for the intensity gain. The increase of the horizontal divergence of the scattered beam, $0.43 / 0.0058 = 7.4$, is the predominant factor in the obtained gain of intensity.

5. From the comparison of Fig. 10 and 11 a better signal to background ratio in the focusing case may be noted. No special efforts for reducing the background were performed in both settings of the diffractometer.

6. As was underlined in Section II, the focusing principle holds also for the single-crystal samples. Indeed, the resolution of the peaks obtained from various single crystals agrees well with that for the powdered samples. A remarkable increase of intensity was also observed.

VI. Conclusions.

The following main conclusions may be drawn from the obtained results:

1. The validity of the formulae for a focused diffractometer derived in paper /2/ has been proved experimentally. A good agreement between calculated and measured values of resolution and intensity has been obtained.

2. It has been shown that the intensity measured by means of the focused diffractometer is much higher (at least by an order of magnitude) than the intensity measured with the same resolution using a diffractometer with collimators.

It is easy to calculate that for the same intensity the resolution of the focused diffractometer can be much higher than resolution of the diffractometer with collimators. For example, for the same dimensions of the source, the sample and the counter, the same angles $\alpha_{r0}, \alpha_{s0}, \alpha_{c0}$ and θ_r as used throughout this paper, focusing allows to increase the distances L_r and L_c by a factor of $\sqrt[4]{40} = 2.5$ (vacuum neutron guides must be used!) with no change in intensity. This would be accompanied by decrease of the halfwidths by the same factor 2.5 to the value of 0.6% for 1Å and 0.2% for 4Å.

By the way the validity of the main principles for resolution and intensity calculations outlined in paper /6/ have been proved experimentally.

The authors wish to thank Professor Bronisław Buras for discussion and many valuable remarks. Dr. V.V. Nitc is thanked for his collaboration in the reconstruction of the diffractometer.

Appendix

Following the main results described in paper /6/ formulae will be derived for the partial resolution D_c^2 due to dimensions of the counter and for the partial resolution D_s^2 due to dimensions of the powdered sample.

1. Assuming homogeneity of the scintillator, D_c^2 is expressed in terms of integrals over the volume of the scintillator:

$$D_c^2 = \int r_c^2 d_3 \vec{r}_c / \int d_3 \vec{r}_c \, , \tag{A1}$$

where

$r_c = \vec{\rho}_c \vec{r}_c$ (according to formula (3)),

$\vec{\rho}_c$ is given by formula (9), and

$\overline{\vec{r}_c} = 0$ is achieved by an appropriate choice of the origin of the coordinate system.

As in the described experiment, the counter which surface is a rectangle parallel to the z_c axis, is considered. Therefore the problem may be reduced to one-dimensional, since the z_c-component of $\vec{\rho}_c$ equals zero.

$$D_c^2 = \frac{1}{\Delta w_c} \int_{-\Delta w_c/2}^{+\Delta w_c/2} \rho_c^2 \cos^2[\alpha_{c0} - (\alpha_c - \pi/2)] \, w^2 \, dw =$$

$$= \frac{1}{12}\left[\frac{\cot^2\theta}{4} + \left(\frac{p}{1+p}\right)^2\right] \sin^2(\alpha_c - \alpha_{c0}) \left(\frac{\Delta w_c}{L_c}\right)^2 \, . \tag{A2}$$

where Δw_c is the width of the counter (a dimension in the direction perpendicular to the z_c-axis).

Formula (A2) was derived under the assumption that the divergence of the beam of the registered neutrons is limited by the size of the counter. In the case when an additional diafragma (shielding) restricts the divergence of the neutron beam to the value ω_c, formula (A2) is replaced by

$$D_c^2 = \frac{1}{12}\left[\frac{\cot^2\theta}{4} + \left(\frac{p}{1+p}\right)^2\right] \frac{\sin^2(\alpha_c - \alpha_{c0})}{\cos^2(\alpha_c)} \, \omega_c^2 \tag{A3}$$

It follows immediately from formula (A2) when the divergence of the beam corresponding to the counter width is substituted:

$$\omega_c = \cos\alpha_c \, \Delta w_c / L_c \, . \tag{A4}$$

2. The formula for D_s^2 may be derived in a similar way as in the case of the counter. Neglecting absorption in the sample, resolution is given by the formula:

$$D_s^2 = \int r_s^2 d_3 \vec{r}_s / \int d_3 \vec{r}_s \tag{A5}$$

where, according to formula (3)

$r = \vec{\rho}_s \vec{r}_s$, and

$\vec{\rho}_s$ is given by formula (10)

$\overline{r_s} = 0$ by an appropriate choice of the origin of the coordinate system.

The sample has a form of a rectangular parallelepiped with one edge parallel to the z_s-axis. Let $\vec{R}_s = (X_s, Y_s, Z_s)$ be a coordinate connected with the sample, X_s-axis is along one (longer) side, and Y_s - axis is along the other side, $Z_s = z_s$ - axis is perpendicular to the scattering plane. The sample is turned around Z_s axis by the angle α_s with respect to the (x_s, y_s, z_s) coordinate system (see Fig. 7 and compare with Fig. 2). Then

$$r_s^2 = (\vec{R}_s \cdot \vec{\rho}_s)^2 = [Y_s \cdot |\vec{\rho}_s| \cdot \cos(\alpha_{s0} - \alpha_s) + X_s |\vec{\rho}_s| \sin(\alpha_{s0} - \alpha_0)]^2 \tag{A6}$$

and finally

$$D_s^2 = \int (\vec{R}_s \vec{\rho}_0)^2 d_3 \vec{R}_s / \int d_3 \vec{R}_s = \frac{1}{12} \rho_s^2 [\Delta Y_s^2 \cos^2(\alpha_{s0} - \alpha_s) + \Delta X_s^2 \sin^2(\alpha_{s0} - \alpha_s)] , \tag{A7}$$

where

ΔX_s and ΔY_s denote the length and the thickness of the sample, respectively,

$$\rho_s^{2} = \left[\frac{\cos\theta_0 \,(p - 1/p)}{2(L_r + L_c)\cos\alpha_{s0}} \right]^2 ,$$

according to formulae (10) and (14).

R e f e r e n c e s

1. B. Buras. Application of Repetitively Pulsed Reactors to Structure and Dynamics Studies of Solids; in Research Applications of Nuclear Pulsed Systems, Proceedings of a Panel, Dubna, 18-22 July 1966; IAEA, Vienna 1967. This paper includes an extendent list of references regarding the TOF diffractometry.
2. A. Holas. Focusing of the Time-of-Flight Diffractometer for Structure Analysis. Report of the Institute of Nuclear Research, INR Nr 742 / II/ PS, Warsaw 1966, and to be published in Nukleonika.
3. Г.Е.Блохин и др. Атомная энергия, 10, 437 (1961).
4. В.В. Нитц, З.Г. Папулова, И. Сосновска, Е. Сосновски. ФТТ, 6, 1369 (1964).
5. В.В. Нитц, И. Сосновска, Е. Сосновски, Ф.Л. Шапиро. Препринт ОИЯИ 2081, Дубна 1965.
6. B. Buras, A. Holas. Intensity and Resolution in the Time-of-Flight Powder Diffractometry. Report of the Institute of Nuclear Research, INR Nr 745 / II/ PS Warsaw 1966, and to be published in Nukleonika.

Received by Publishing Department
on March 7, 1968.

Table I

The gain of intensity in the focused spectrometer
as compared with the spectrometer with collimators

$hk\ell$	33I	400	3II	220	III
λ in $\mathring{A}$	I.72	I.88	2.26	2.65	4.33
I_f / I_o	35	33	23.4	I9.9	7.7
I_f / I_c corrected	47	49	39	38	36

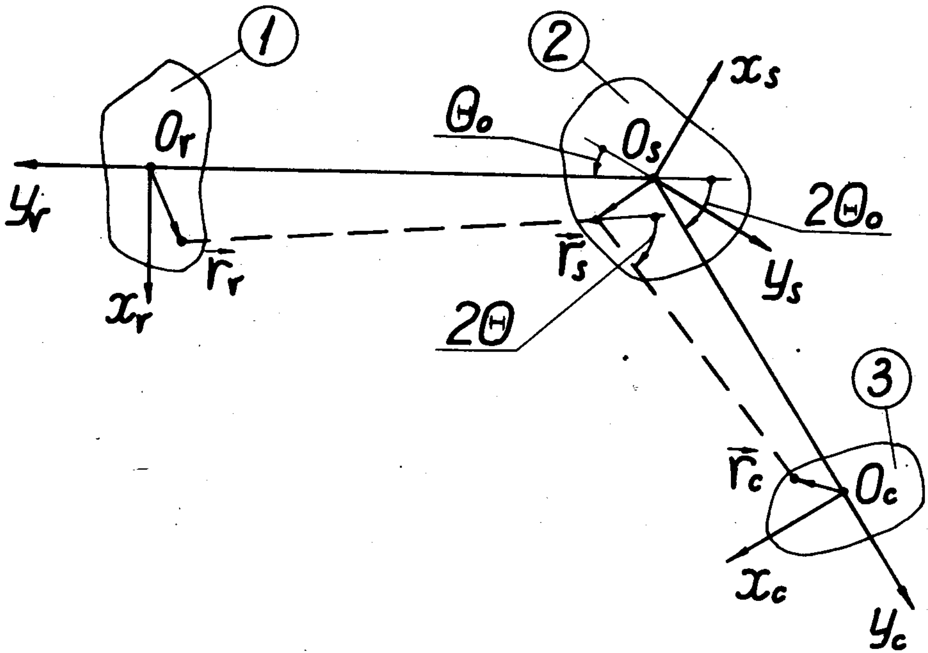

Fig. 1. The scheme of the time-of-flight spectrometer: source (1), sample (2), counter (3). The axes z_r, z_s, z_c are going through the points O_r, O_s, O_c, respectively, perpendicular to the figure plane.

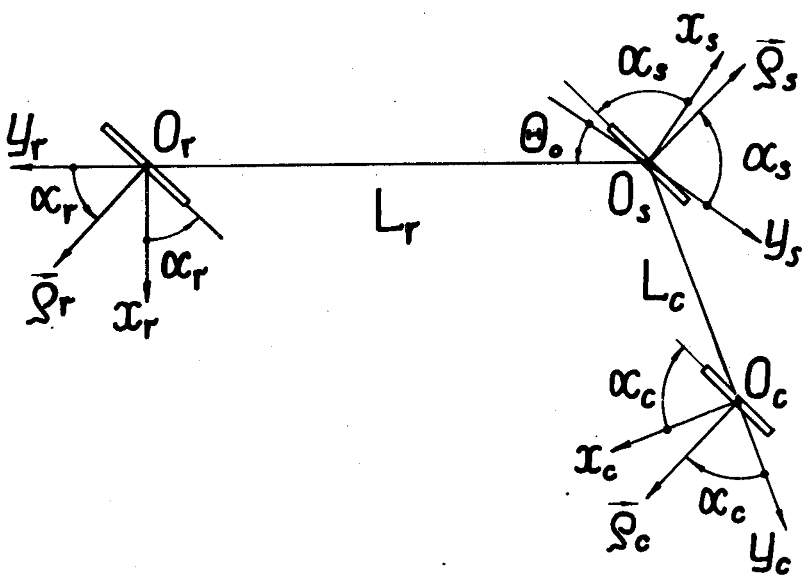

Fig. 2. The scheme of the focused spectrometer. As an example, we took $\theta_0 = 35^\circ$, $p = 1/2$. Corresponding focusing angles $\alpha_r = \alpha_{r0} = 47^\circ$, $\alpha_s = \alpha_{s0} = 81^\circ$ and $\alpha_c = \alpha_{c0} = 65^\circ$ are drawn.

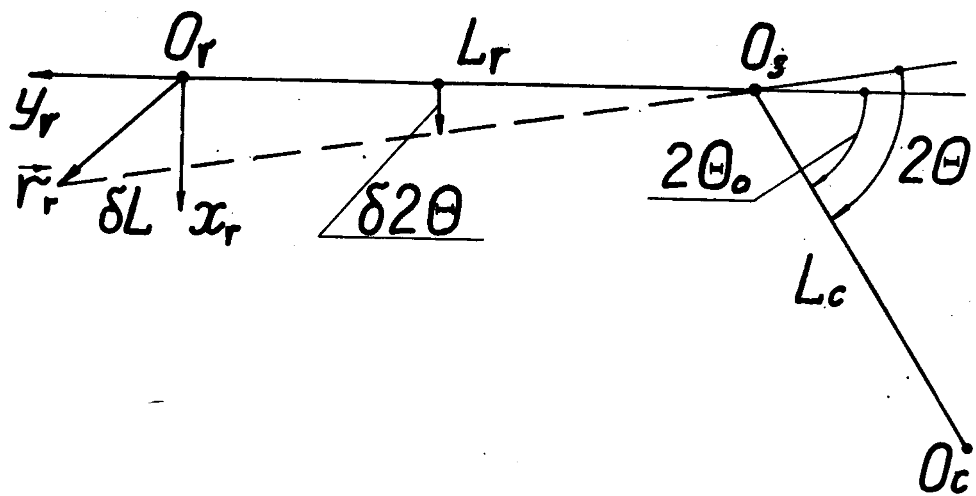

Fig. 3. The scheme for focusing calculation of the source.

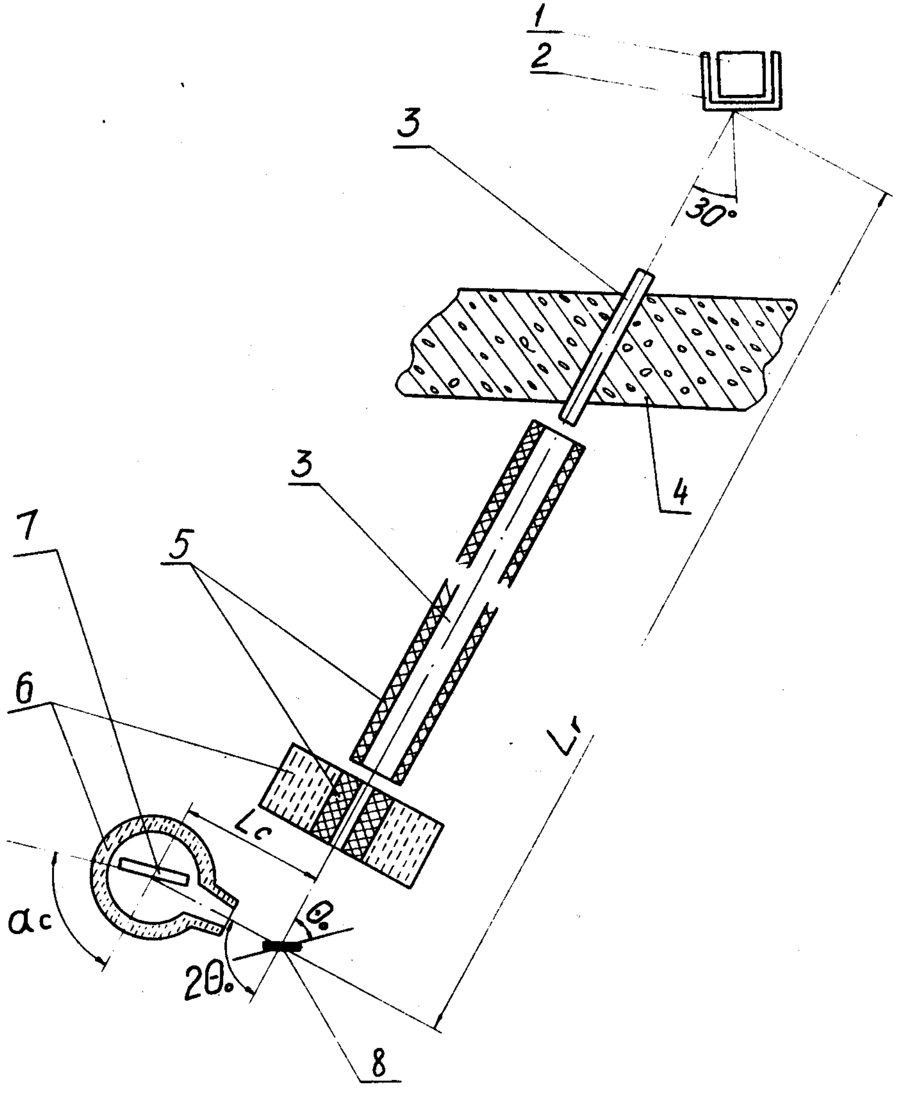

Fig. 4. The scheme of the spectrometer at IBR in Dubna: reactor core (1), moderator (2), neutron guides (2), wall of the reactor hall (4), borated paraphine shielding (5), water shielding (6), counter (7), sample (8).

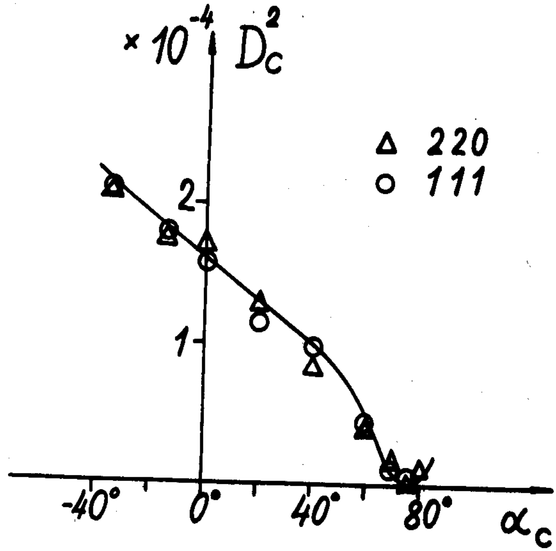

Fig. 5. The resolution due to the counter width vs inclination angle of the counter.

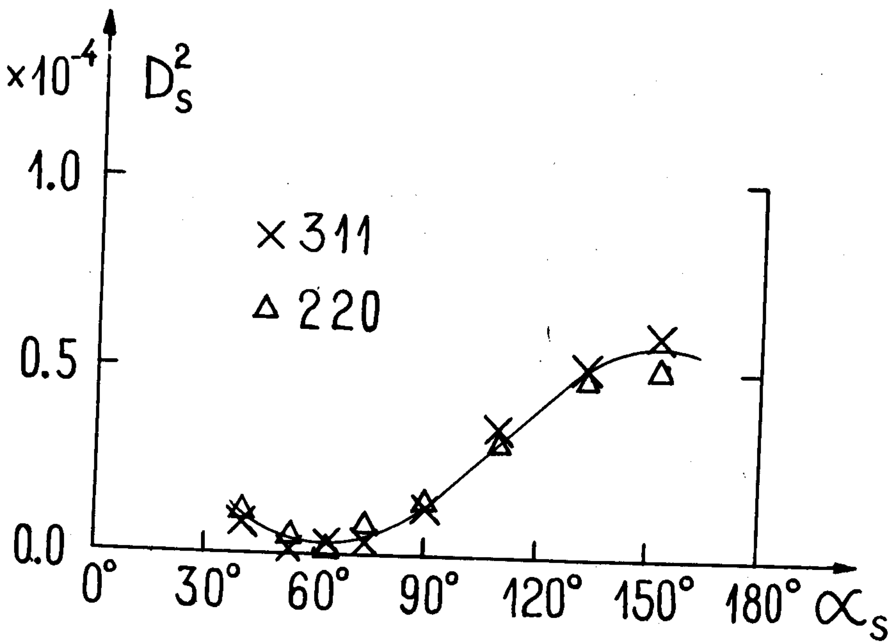

Fig. 6. The resolution due to the sample dimensions vs azymuthal angle of the sample.

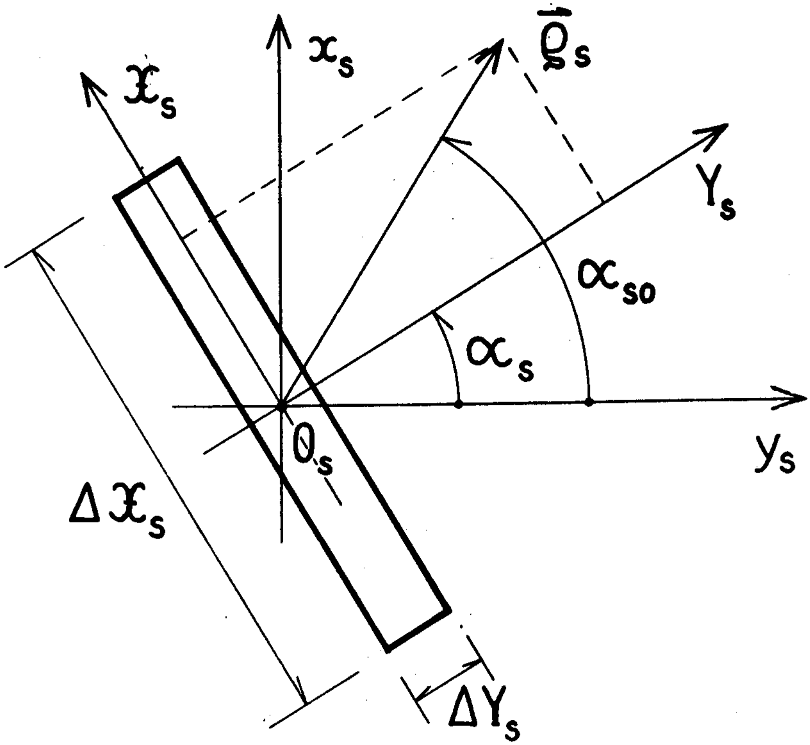

Fig. 7. The scheme for calculations of the resolution due to the sample.

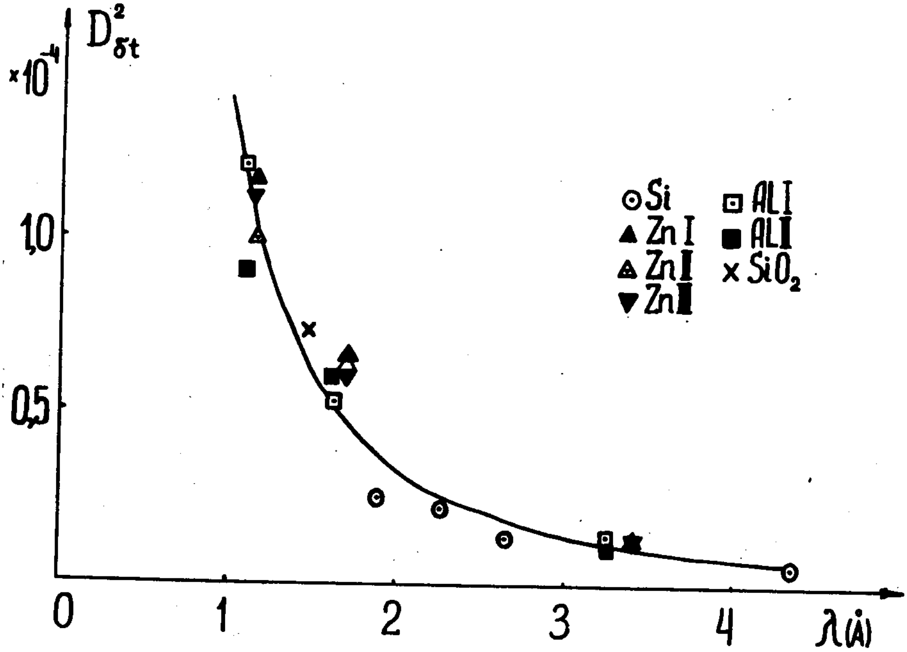

Fig. 8. The resolution in the focusing conditions.

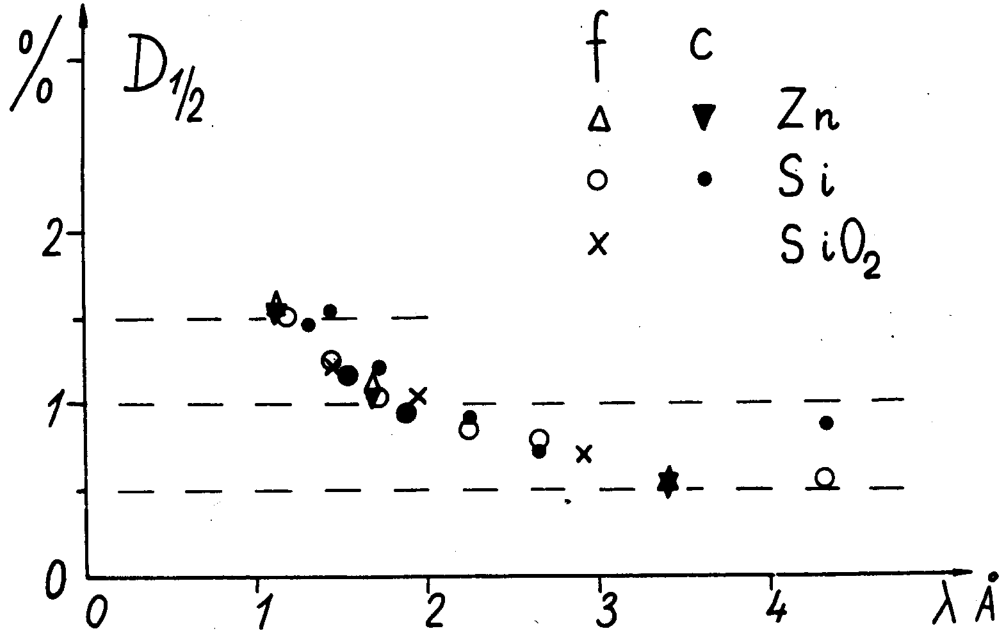

Fig. 9. Halfwidth of the peaks obtained with the focused diffractometer ("f") and with the diffractometers with collimators ("c").

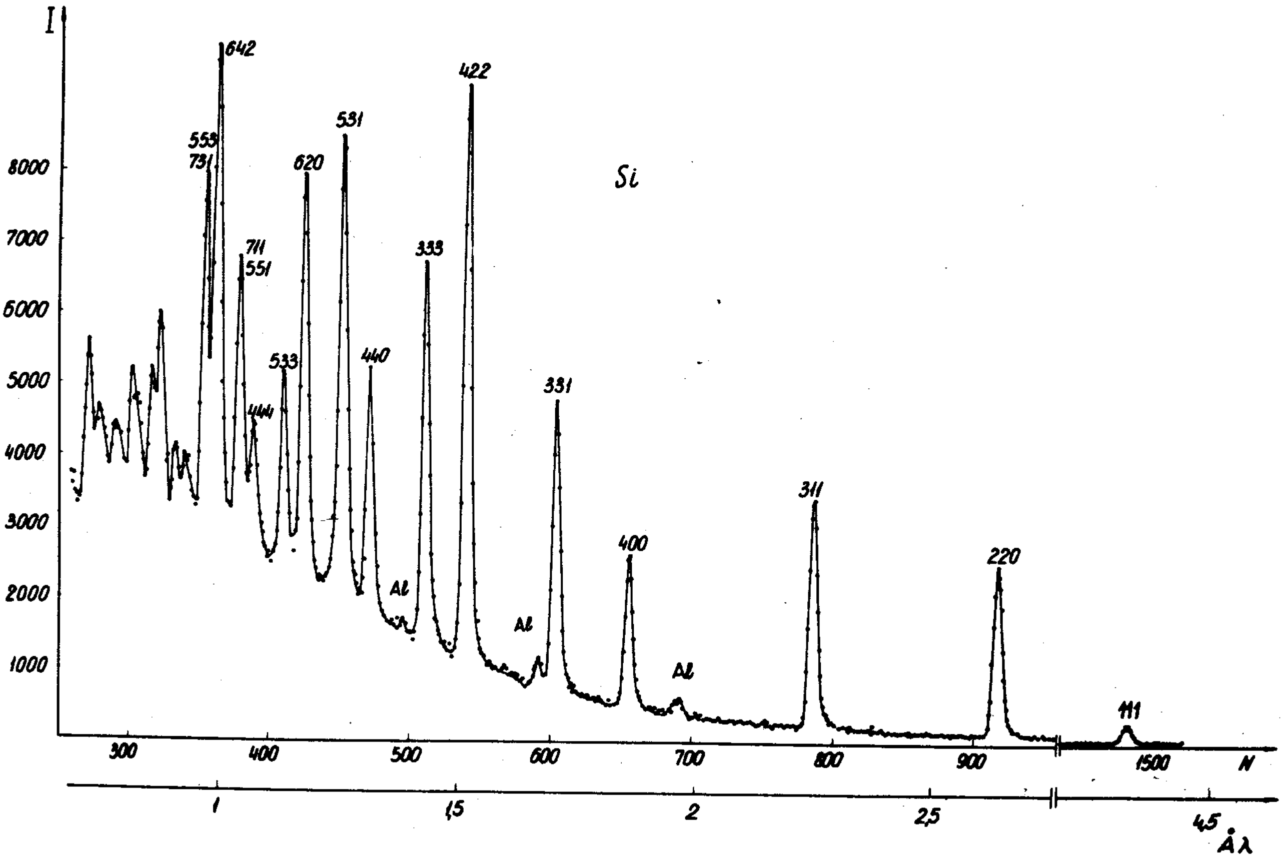

Fig. 10. The diffraction pattern of powdered Si using the focused diffractometer.

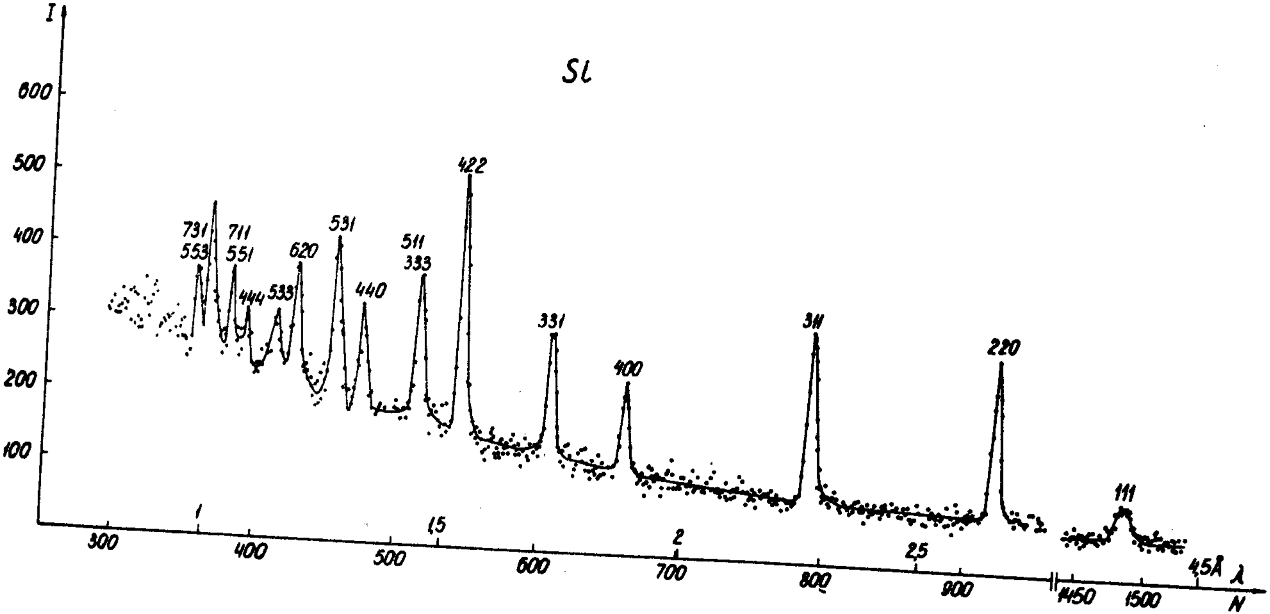

Fig. 11. The diffraction pattern of powedered Si using the diffractometer with collimators.

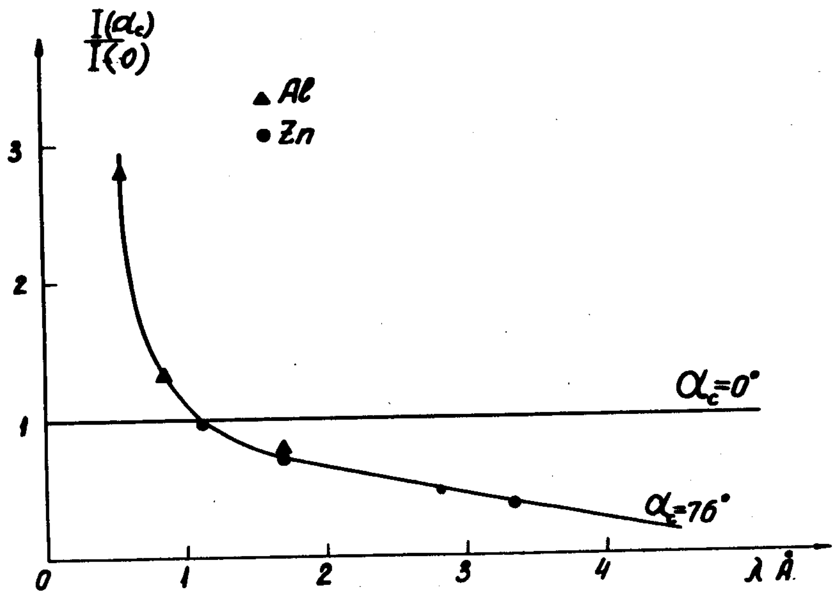

Fig. 12. The intensity measured by the declined counter as a function of the wavelength.